# Impurity-induced resonant Raman scattering

C. Trallero-Giner,* A. Cantarero,† and M. Cardona
*Max-Planck-Institut für Festkörperforschung, Heisenbergstrasse 1, Postfach 80 05 65, D-7000 Stuttgart 80, Federal Republic of Germany*

M. Mora
*Department of Theoretical Physics, Havana University, San Lázaro y L, Havana, Cuba*
(Received 17 October 1991; revised manuscript received 28 January 1992)

An explicit expression for impurity-induced one-LO-phonon forbidden resonant Raman scattering in diamond and zinc-blende-type semiconductors, which includes excitonic effects, is presented. It is derived by fourth-order perturbation theory and can be applied in a photon energy range below and above the exciton energy. We have considered both neutral and ionized impurities in the exciton-impurity coupling. Discrete and continuous exciton states have been taken as virtual intermediate states in the process, and the matrix elements corresponding to different excitonic transitons have been calculated analytically. The different contributions to the squared Raman polarizability are compared; the most important ones are found to be due to discrete-discrete-discrete transitions. An analysis of the dependence of the Raman-scattering efficiency on impurity concentration, screening factor, and lifetime broadening is presented and quantitative differences with the forbidden Fröhlich Raman scattering by LO phonons are discussed. These results are used to calculate the absolute value of the Raman efficiency around the $E_0$ gap of AlSb and the $E_0+\Delta_0$ gap of GaAs. The actual role of the impurity-induced scattering in terms of the impurity concentration is clarified.

## I. INTRODUCTION

Dipole-forbidden Raman scattering by LO phonons has been reported in several III-V and II-VI compound semiconductors.[1–12] This Raman process was observed in CdS.[13,14] The electrons and holes can interact via the Fröhlich mechanism leading to a diagonal Raman tensor for transitions near $\mathbf{k} \simeq 0$ in cubic semiconductors. This forbidden scattering can be observed in the backscattering configuration $z(x,x)\bar{z}$ for a (001) surface ($x \parallel [100]$, $y \parallel [010]$, $z \parallel [001]$ directions) in the zinc-blende-type semiconductors. Crystal momentum conservation implies that the phonon wave vector $\mathbf{q} = \kappa_l - \kappa_s$, $\kappa_l$ and $\kappa_s$ being the wave vector of the incident and scattered photons, respectively. In the dipole approximation ($\mathbf{q} = 0$) the Raman process is forbidden. In Ref. 15 it was shown that the finiteness of the photon wave vector makes the process "allowed" and thus, a strongly one-phonon Raman efficiency is obtained. Consequently, in the past, several papers have appeared where absolute values of Raman scattering efficiency or Raman polarizability arising from intraband Fröhlich ($F$) electron-phonon interaction and its interference with the corresponding allowed scattering due to the deformation-potential (DP) mechanism have been reported[2–12] in different backscattering configurations.

Recently, the role of excitons in one-phonon Raman processes in III-V compounds has been clarified.[16–19] The theory developed for short-range interband scattering[16] and long-range intraband scattering,[17] taking into account excitonic effects, reproduces the experimental absolute values of squared Raman polarizabilities as well as the resonance profiles. Another contribution to the forbidden Raman scattering by LO phonons involving impurities was proposed in Ref. 20. A model, assuming free-electron-hole pairs (uncorrelated theory) and including scattering by ionized impurities, was given in Ref. 3. That model was developed keeping in mind the similarity of the extrinsic mechanism with the scattering by two-phonons process,[21] where one of the emitted phonons is replaced by the ionized impurity. Following this idea, it was claimed in several papers (see, for instance, Refs. 3, 5, 8, and 9) that the extrinsic impurity-induced scattering plays a dominant role with respect to the long-range Fröhlich intraband mechanism even in nominally high-purity samples. The spectra of GaAs around the $E_0+\Delta_0$ gap were fitted[5] with this uncorrelated electron-hole theory and assuming that 50–70% of the total scattering amplitude is due to extrinsic impurity scattering. The authors of Ref. 8 added 70% of impurity-induced scattering in order to fit the experimental data of GaSb in the neighborhood of the $E_0+\Delta_0$ critical point (CP).

The theory of one-phonon resonant Raman scattering including excitonic effects[17,18] shows that the impurity mechanism is not as important as previously assumed, even at the $E_0+\Delta_0$ CP.[18] The Raman profile of the GaP at $E_0$ and $E_0+\Delta_0$ CP's, the GaSb at the $E_0+\Delta_0$ gap, and also the $E_0+\Delta_0$ CP of GaAs for different temperatures were fitted for the $F$ interaction and its interference with DP mechanism[18] calculated using the correlated electron-hole-pair theory. No assumption of impurity-induced forbidden scattering was necessary to reproduce the experimental data and to reach the measured absolute values in these III-V compounds. Nevertheless,

 

some experimental evidence shows that for moderately high impurity concentration [for example, in commercial samples with $10^{16}$ donors/cm$^3$ (Refs. 3 and 18)] an impurity-induced increase in forbidden scattering should be observed. Recent measurements in AlSb (Ref. 22) show that in the $z(x,x)\bar{z}$ geometry, the Raman efficiencies measured at high temperatures are stronger than at low temperatures, a fact that can be explained if an additional mechanism involving scattering of excitons by impurities is added to the $F$ interaction. Such a mechanism should be stronger at high temperatures, when impurities are ionized. These remarks emphasize the need for an excitonic treatment of the impurity-induced scattering.

In Ref. 20 a calculation of the impurity-induced LO-phonon Raman scattering was presented considering only the exciton ground state $n = 1$ for a laser frequency above the gap and approximate analytical expressions for the Raman tensor were obtained. This result cannot be used to elucidate quantitatively the principal features of the Raman scattering efficiencies. Moreover, transitions between the discrete and continuous exciton states give the principal contribution to the first- and second-order Raman scattering when the Fröhlich interaction is considered.[17,23]

In this paper we present an excitonic treatment of the impurity-induced LO-phonon resonant Raman scattering valid in a broad spectral range around direct allowed excitonic transitions. The fundamental relations for this process are summarized in Sec. II. Section III is devoted to the calculation of the Raman tensor and the impurity concentration and excitonic broadening effects are analyzed. In Sec. IV this theory is compared to experiments for GaAs around the $E_0 + \Delta_0$ CP and for AlSb near the $E_0$ gap. Section V summarizes the main conclusions of the work.

## II. FUNDAMENTAL RELATIONS

To calculate the Raman scattering efficiency we choose a two-band model with isotropic parabolic bands and correlated electron-hole pairs as excited states in the framework of the Wannier-Mott effective-mass approximation. If the polariton effect is neglected, the main diagrams contributing to the impurity-induced LO-phonon Raman scattering are shown in Fig. 1. The process is described in the following way: a virtual exciton in the state $\alpha$ with center of mass wave vector $\mathbf{K} = \boldsymbol{\kappa}_l$ is created by the incident light; the exciton is scattered by an impurity center making a transition to the state $\beta$, $\mathbf{K} = \mathbf{q} + \boldsymbol{\kappa}_s$ [see Fig. 1(a)], the impurity transfers a wave vector $\mathbf{q} + \boldsymbol{\kappa}_s - \boldsymbol{\kappa}_l$ to the excitonic state; the exciton emits one LO phonon with frequency $\omega_{\mathrm{LO}}$ and wave vector $\mathbf{q}$ and changes its state to $\gamma$ and $\mathbf{K} = \boldsymbol{\kappa}_s$; finally, the virtual exciton recombines and a scattered photon with frequency $\omega_s = \omega_l - \omega_{\mathrm{LO}}$ is emitted.

Another contribution to the Raman efficiency arises from the permutation of $H_{\text{exc-}i}$ and $H_{\text{exc-ph}}$ [Fig. 1(b)]

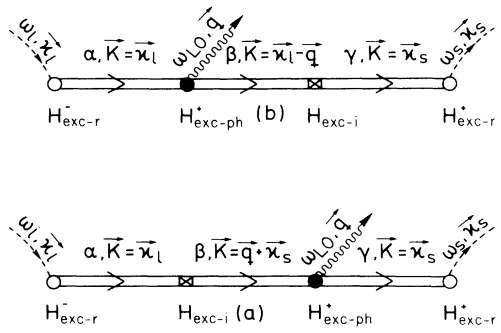


FIG. 1. Diagrams contributing to impurity-induced 1LO-phonon Raman scattering. $H^{\pm}_{\text{exc-}r}$, $H_{\text{exc-}i}$, and $H^{+}_{\text{e-ph}}$ represent the exciton-radiation, exciton-impurity, and exciton-phonon Fröhlich interactions, respectively.

Hamiltonians defined below, and the interpretation is the same as given in the above case. In both Feynman diagrams the quasimomentum conservation is relaxed and phonons with $\mathbf{q} \neq \boldsymbol{\kappa}_l - \boldsymbol{\kappa}_s$ can participate in the Raman process. This scattering process can be treated in fourth-order perturbation theory with two crystal-radiation interactions, one exciton-phonon interaction, and one exciton-impurity interaction vertex.

### A. Hamiltonian of the system

The total Hamiltonian is given by

$$H = H_0 + H_{\text{exc-}r} + H_{\text{exc-ph}} + H_{\text{exc-}i} \ , \tag{1}$$

where $H_{\text{exc-}r}$, $H_{\text{exc-ph}}$, and $H_{\text{exc-}i}$ are the exciton-photon, exciton-phonon, and exciton-impurity interaction Hamiltonians, respectively. Here we are interested in the intraband Fröhlich Hamiltonian, i.e., $H_{\text{exc-ph}} = H_{\text{exc-}F}$. In Eq. (1), $H_0$ is the unperturbed Hamiltonian which can be written as

$$H_0 = \sum_{\boldsymbol{\kappa},\mathbf{e}} \hbar\omega(a^{\dagger}_{\boldsymbol{\kappa},\mathbf{e}} a_{\boldsymbol{\kappa},\mathbf{e}} + \tfrac{1}{2}) + \sum_{\nu,\mathbf{q}} \hbar\omega_{\nu}(\mathbf{q})(b^{\dagger}_{\mathbf{q},\nu} b_{\mathbf{q},\nu} + \tfrac{1}{2})$$

$$+ \sum_{\mathbf{K},\lambda} E_{\lambda,\mathbf{K}}(d^{\dagger}_{\lambda,\mathbf{K}} d_{\lambda,\mathbf{K}} + \tfrac{1}{2}) \ , \tag{2}$$

corresponding to the free-photon, phonon, and exciton field, respectively, where $a_{\boldsymbol{\kappa},\mathbf{e}}$ represents the annihilation operator of a photon with wave vector $\boldsymbol{\kappa}$, polarization $\mathbf{e}$, and frequency $\omega$, $b_{\mathbf{q},\nu}$ the annihilation operator of a phonon with wave vector $\mathbf{q}$ belonging to the branch $\nu$ and phonon frequency $\omega_{\nu}$; $d_{\lambda,\mathbf{K}}$ the exciton annihilation operator with internal quantum number $\lambda$, center-of-mass wave vector $\mathbf{K}$, and energy $E_{\lambda,\mathbf{K}}$ given by

$$E_{\lambda,\mathbf{K}} = E_g + \frac{\hbar^2 K^2}{2m_E} - \frac{R}{n^2} \quad (n = 1, 2, ...) \tag{3}$$

for the discrete spectrum, and

$$E_{\lambda,\mathbf{K}} = E_g + \frac{\hbar K^2}{2m_E} + \frac{\hbar^2 k_E^2}{2\mu} \tag{4}$$

for the continuum. Here $E_g$ is the energy gap, $m_E = m_e + m_h$, $m_e$ ($m_h$) is the electron (hole) effective mass, $R$ is the exciton Rydberg, $\mu$ is the reduced mass, $k_E$ is the exciton wave vector. Furthermore we have

$$H_{\text{exc-}r} = \sum_{\mathbf{K},\lambda} \sum_{\boldsymbol{\kappa},\mathbf{e}} T_\lambda(\mathbf{K})(d^\dagger_{\lambda,\mathbf{K}} + d_{\lambda,\mathbf{K}})a_{\boldsymbol{\kappa},\mathbf{e}} + \text{H.c.} \tag{5}$$

$T_\lambda(\mathbf{K})$, the exciton-photon coupling constant, for direct allowed transition is given by[24]

$$T_\lambda(\mathbf{K}) = -\frac{e}{m}\sqrt{\frac{2\pi\hbar}{\omega\eta^2}}\mathbf{e}\cdot\mathbf{p}_{cv}\varphi_\lambda(0)\delta_{\mathbf{K},\boldsymbol{\kappa}} , \tag{6}$$

where $\mathbf{p}_{cv}$ is the matrix element of the momentum operator, $\eta$ the refractive index, and $\varphi_\lambda(\mathbf{r})$ the wave function of the internal exciton state. The exciton-phonon interaction Hamiltonian is expressed by

$$H_{e\text{-}F} = \sum_{\mathbf{q},\nu} \sum_{\lambda,\lambda'} \sum_{\mathbf{K},\mathbf{K}'} [S^{\mathbf{K}',\mathbf{K}}_{\lambda',\lambda}(\mathbf{q}) d^\dagger_{\lambda',\mathbf{K}'} d_{\lambda,\mathbf{K}} b^\dagger_{\mathbf{q},\nu}] + \text{H.c.} \tag{7}$$

The exciton-phonon coupling constant $S^{\mathbf{K}',\mathbf{K}}_{\lambda',\lambda}(\mathbf{q})$ for long-wavelength longitudinal polar-optical phonons (Fröhlich interaction) is given by[25]

$$S^{\mathbf{K}',\mathbf{K}}_{\lambda',\lambda}(\mathbf{q}) = \frac{C^*_F}{q}\left[I^h_{\lambda',\lambda}(-\mathbf{q}) - I^e_{\lambda',\lambda}(\mathbf{q})\right]\delta_{\mathbf{K}',\mathbf{K}-\mathbf{q}} , \tag{8}$$

$$C_F = -i\sqrt{\frac{2\pi\hbar\omega_\nu e^2}{V}\left(\varepsilon_\infty^{-1} - \varepsilon_0^{-1}\right)} , \tag{9}$$

$\varepsilon_0$ and $\varepsilon_\infty$ being the low- and high-frequency permitivities and $V$ the crystal volume. $I^\alpha_{\lambda',\lambda}(\mathbf{q})$ ($\alpha = e, h$) is the matrix element between internal exciton states $\lambda, \lambda'$ defined as

$$I^\alpha_{\lambda',\lambda}(\mathbf{q}) = \int d^3\mathbf{r}\,\varphi^*_{\lambda'}(\mathbf{r}) e^{i(m_\alpha/m_E)\mathbf{q}\cdot\mathbf{r}}\varphi_\lambda(\mathbf{r}). \tag{10}$$

The exciton-impurity interaction Hamiltonian can be written as

$$H_{\text{exc-}i} = \sum_{\mathbf{q}} \sum_{\lambda,\lambda'} \sum_{\mathbf{K},\mathbf{K}'} [M^{\mathbf{K}',\mathbf{K}}_{\lambda',\lambda}(\mathbf{q}) d^\dagger_{\lambda',\mathbf{K}'} d_{\lambda,\mathbf{K}}] , \tag{11}$$

where $M^{\mathbf{K}',\mathbf{K}}_{\lambda',\lambda}(\mathbf{q})$ is the exciton-impurity coupling constant:

$$M^{\mathbf{K}',\mathbf{K}}_{\lambda',\lambda}(\mathbf{q}) = g(\mathbf{q})\left[I^h_{\lambda',\lambda}(-\mathbf{q}) - I^e_{\lambda',\lambda}(\mathbf{q})\right]\delta_{\mathbf{K}',\mathbf{K}-\mathbf{q}} , \tag{12}$$

and $g(\mathbf{q})$ is the impurity vertex which depends on the kind of impurity under consideration (see Appendix A).

### B. Raman scattering efficiency

The differential cross section $d\sigma/d\Omega$, the Raman scattering efficiency per unit length and unit solid angle $d\Omega$, for fixed final phonon brach $\nu$, $dS/d\Omega$ and the scattering amplitude $W_{\text{FI}}$ are related, for a Stokes process, through the equation

$$\frac{1}{V}\frac{d\sigma}{d\Omega} = \frac{dS}{d\Omega} = \frac{\omega_l\omega_s^3}{(2\pi)^2}\frac{\eta_l\eta_s^3}{c^4}\frac{V}{(\hbar\omega_l)^2} \times \sum_F |W_{\text{FI}}(\omega_s, \mathbf{e}_s; \omega_l, \mathbf{e}_l)|^2[N(\omega_{\text{LO}}) + 1] , \tag{13}$$

where $|I\rangle$ and $|F\rangle$ are the initial and final states corresponding to the scattering of a photon of frequency $\omega_l$ and polarization $\mathbf{e}_l$ by an LO phonon, giving a scattered photon of frequency $\omega_s = \omega_l - \omega_{\text{LO}}$ and polarization $\mathbf{e}_s$. $N(\omega_{\text{LO}})$ is the Bose-Einstein occupation number for LO phonons in thermal equilibrium at a temperature $T$, and $c$ the speed of light. In the following the indices $l$ and $s$ refer always to incoming and scattered light, respectively. In many III-V (Refs. 2–8) and II-VI (Refs. 9–12) compound semiconductors the scattering efficiency has been given in terms of absolute values of the squared Raman polarizability $\mathsf{a}$ which is related to the Raman tensor $\overleftrightarrow{\mathrm{R}}$ through $\mathsf{a} = \mathbf{e}_s\cdot\overleftrightarrow{\mathrm{R}}\cdot\mathbf{e}_l$ and to the scattering efficiency by the equation

$$\frac{dS}{d\Omega} = \frac{\omega_s^3\omega_l}{c^4}\frac{\hbar}{2V_c M\omega_{\text{LO}}}\sum_F |\mathbf{e}_s\cdot\overleftrightarrow{\mathrm{R}}\cdot\mathbf{e}_l|^2[N(\omega_{\text{LO}}) + 1] , \tag{14}$$

where $V_c$ is the volume of the primitive cell, and $M$ the reduced mass of the atoms in that cell. By comparing Eqs. (13) and (14) the Raman polarizability is obtained in terms of the microscopic amplitude probability $W_{\text{FI}}$. According to the Feynman diagrams in Figs. 1(a) and 1(b), the first-order Raman scattering via impurity-induced Fröhlich interaction is a fourth-order perturbation theory process. Considering only the resonant terms and Eqs. (1)–(12), the scattering amplitude can be expressed as

$$W_{\mathrm{FI}} = \sum_{\alpha,\beta,\gamma} \left( \frac{\langle \hbar\omega_l | H_{\text{exc-}r} | \alpha, \mathbf{K}=0 \rangle \langle \alpha, \mathbf{K}=0 | H_{\text{exc-}i} | \beta, \mathbf{K}=\mathbf{q} \rangle}{(\hbar\omega_l - E_\alpha + i\Gamma_\alpha)\left(\hbar\omega_l - E_\beta - \frac{\hbar^2 q^2}{2m_E} + i\Gamma_\beta\right)} \times \frac{\langle \beta, \mathbf{K}=\mathbf{q} | H_{e\text{-}F} | \gamma, \mathbf{K}=0 \rangle \langle \gamma, \mathbf{K}=0 | H_{\text{exc-}r} | \hbar\omega_s \rangle}{\hbar\omega_s - E_\gamma + i\Gamma_\gamma} + \frac{\langle \hbar\omega_l | H_{\text{exc-}r} | \alpha, \mathbf{K}=0 \rangle \langle \alpha, \mathbf{K}=0 | H_{e\text{-}F} | \beta, \mathbf{K}=\mathbf{q} \rangle}{(\hbar\omega_l - E_\alpha + i\Gamma_\alpha)\left(\hbar\omega_s - E_\beta - \frac{\hbar^2 q^2}{2m_E} + i\Gamma_\beta\right)} \times \frac{\langle \beta, \mathbf{K}=\mathbf{q} | H_{\text{exc-}i} | \gamma, \mathbf{K}=0 \rangle \langle \gamma, \mathbf{K}=0 | H_{\text{exc-}r} | \hbar\omega_s \rangle}{\hbar\omega_s - E_\gamma + i\Gamma_\gamma} \right) . \tag{15}$$

The states $|\lambda\rangle$ ($\lambda = \alpha, \beta, \gamma$) refer to excitonic intermediate states with energy $E_\lambda$ and lifetime broadening $\Gamma_\lambda$. In Eq. (15) $\kappa_l \approx \kappa_s \approx 0$ has been assumed. According to Eqs. (5)–(12), the scattering amplitude can be written as

$$W_{\mathrm{FI}} = R_{ls} \frac{g(\mathbf{q})}{q} \sum_{\alpha,\beta,\gamma} \frac{\varphi^*_\alpha(0)[I^h_{\alpha,\beta}(-\mathbf{q}) - I^e_{\alpha,\beta}(\mathbf{q})][I^h_{\beta,\gamma}(\mathbf{q}) - I^e_{\beta,\gamma}(-\mathbf{q})]\varphi_\gamma(0)}{(\hbar\omega_l - E_\alpha + i\Gamma_\alpha)(\hbar\omega_s - E_\gamma + i\Gamma_\gamma)} \times \left( \frac{1}{\hbar\omega_l - E_\beta - \frac{\hbar^2 q^2}{2m_E} + i\Gamma_\beta} + \frac{1}{\hbar\omega_s - E_\beta - \frac{\hbar^2 q^2}{2m_E} + i\Gamma_\beta} \right) , \tag{16}$$

where

$$R_{ls} = \langle c | \mathbf{e}^*_l \cdot \mathbf{p}^* | v \rangle \langle v | \mathbf{p} \cdot \mathbf{e}_s | c \rangle C^*_F \left(\frac{e}{m}\right)^2 \frac{2\pi\hbar}{\eta_l \eta_s \sqrt{\omega_l \omega_s}} . \tag{17}$$

The first term in the large parentheses of Eq. (16) corresponds to diagram (a) in Fig. 1, i.e., the exciton intermediate transition $|\alpha, \mathbf{K}=0\rangle \rightarrow |\beta, \mathbf{K}=\mathbf{q}\rangle$ due to the interaction with impurities, while the second term represents the contribution to $W_{\mathrm{FI}}$ of diagram (b) in Fig. 1 when the exciton is scattered firstly by a LO phonon. It can be seen from Eq. (16) that terms arising from the permutation of $H_{\text{exc-}i}$ and $H_{e\text{-}F}$ enter differently in the amplitude calculation. In order to evaluate Eq. (16) it is necessary to know the matrix elements $I_{\alpha,\beta}(\mathbf{q})$ between different exciton states, i.e., transitions between discrete-discrete, discrete-continuous, and continuous-continuous states. In a one-phonon process (without impurity interaction) only the $s$-exciton states (angular momentum $l = 0$) for discrete and continuum excitations contribute to the scattering efficiency.[16,17] The different matrix elements for exciton transitions with $l = 0$ are reported in Ref. 17. In the case of an impurity-induced LO phonon (or a second-order Raman scattering process) and according to Eq. (16) exciton transitions with angular momentum $l \geq 0$ have to be consider in the scattering amplitude. In the following we consider the Wannier-Mott hydrogenic model in the framework of the envelope-function approximation.

### C. Wave functions and matrix elements

The Wannier-Mott exciton envelope wave functions for the discrete spectrum in spherical coordinates are[26]

$$\varphi_{n,l,m}(r,\theta,\phi) = \frac{2}{n^{l+2}(2l+1)!}\sqrt{\frac{(n+l)!}{a^3(n-l-1)!}}\left(\frac{2r}{a}\right)^l \times e^{-r/an} F\left(-n+l+1, 2l+2; \frac{2r}{an}\right) \times Y_{l,m}(\theta,\phi) , \tag{18}$$

where $F(a,b;z)$ is the confluent hypergeometric function, $Y_{l,m}(\theta,\phi)$ are the spherical harmonics, with $l = 0, 1, \ldots, n-1$, and $m$ runs from $-l$ to $l$, and $a$ is the exciton Bohr radius. For the case $\mathbf{r} = 0$,

$$\varphi_{n,l,m}(0) = \frac{1}{\sqrt{\pi a^3 n^3}} \delta_{l,0}\delta_{m,0} . \tag{19}$$

For the continuous spectrum[26]

$$\varphi_{k,l,m}(r,\theta,\phi) = \frac{1}{\sqrt{V}} \frac{2k}{(2l+1)!} e^{\pi/2k} |\Gamma(l+1-i/k)| \times \left(\frac{2kr}{a}\right)^l e^{-ikr/a} \times F\left(\frac{i}{k}+l+1, 2l+21; \frac{ikr}{a}\right) Y_{l,m}(\theta,\phi) , \tag{20}$$

where $k = k_E a$, and $\Gamma(z)$ is the gamma function. The continuous spectrum is infinitely degenerate, to each value of $E = \hbar^2 k_E^2 / 2\mu$ it corresponds an infinite number of states, with $l$ running from 0 to $\infty$ and $m = 0, \pm 1, \ldots, \pm l$. In the case $\mathbf{r} = 0$

$$\varphi_{k,l,m}(0) = \frac{1}{\sqrt{\pi V}} k e^{\pi/2k} |\Gamma(1+i/k)| \delta_{l,0}\delta_{m,0} . \tag{21}$$

For simplicity, in the calculation of the continuous-

continuous matrix elements we take for the exciton the uncorrelated electron-hole pair approximation:[17]

$$\varphi_{\mathbf{k}}(\mathbf{r}) = \frac{1}{\sqrt{V}} e^{i\mathbf{k}\cdot\mathbf{r}/a} . \tag{22}$$

The function $\varphi_{k,l,m}(\mathbf{r})$ [Eq. (20)] is normalized as follows:[26]

$$\int_V \varphi^*_{k,l,m}(\mathbf{r})\varphi_{k',l',m'}(\mathbf{r})d^3\mathbf{r} = 2\pi\frac{a^3}{V}\delta(k-k')\delta_{l,l'}\delta_{m,m'} , \tag{23}$$

while $\varphi_{\mathbf{k}}(\mathbf{r})$ [Eq. (22)] is normalized according to[26]

$$\int_V \varphi^*_{\mathbf{k}'}(\mathbf{r})\varphi_{\mathbf{k}}(\mathbf{r})d^3\mathbf{r} = (2\pi)^3\frac{a^3}{V}\delta(\mathbf{k}-\mathbf{k}') . \tag{24}$$

The matrix elements $I_{\alpha,\beta}(\mathbf{q})$ are evaluated in Appendix B. For discrete-discrete transitions they are given by

$$I_{n,0;n',l'}(Q_\alpha) = C_{n,0;n',l'}Q_\alpha^{l'}\left(\frac{d}{Q_\alpha dQ_\alpha}\right)^{l'} \times\left\{\frac{1}{Q_\alpha}\mathrm{Im}\mathcal{I}_{n,0;n',l'}(Q_\alpha)\right\} , \tag{25}$$

where the constant $C_{n,0;n',l'}$ and the function $\mathcal{I}_{n,0;n',l'}(Q_\alpha)$ are defined in Appendix B, and $\mathbf{Q}_\alpha = (m_\alpha/m_E)\mathbf{q}a$. The $I_{n,0;n',l'}(Q)$ matrix elements satisfy the following properties:

$$\begin{aligned} I_{n',l';n,0}(Q) &= (-1)^{l'} I_{n,0;n',l'}(Q) , \\ I_{n,0;n',l'}(-Q) &= (-1)^{l'} I_{n,0;n',l'}(Q), \\ I_{n',l';n,0}(-Q) &= I_{n,0;n',l'}(Q) . \end{aligned} \tag{26}$$

Figure 2 shows the matrix element as a function of $Q$ for $n$ and $n'$ from 1 to 3 with $l' = 0$ [Fig. 2(a)] and $l' = 1$ [Fig. 2(b)]. From Fig. 2 it can be seen that $I_{n',l';n,0}$ decreases rapidly with increasing $Q$ and for a given $l'$ the maximum contribution comes from $n = n'$.

The discrete-continuous matrix element $I_{n,0;k,l}(Q)$ can be put in the form (see Appendix B)

$$I_{n,0;k,l}(Q) = C_{n,0;k,l}\sqrt{\frac{a^3}{V}}Q^l\left(\frac{d}{QdQ}\right)^l \times\left\{\frac{1}{2iQ}(\mathcal{I}_{n,0;k,l}(Q) - \mathcal{I}_{n,0;k,l}(-Q))\right\} , \tag{27}$$

where

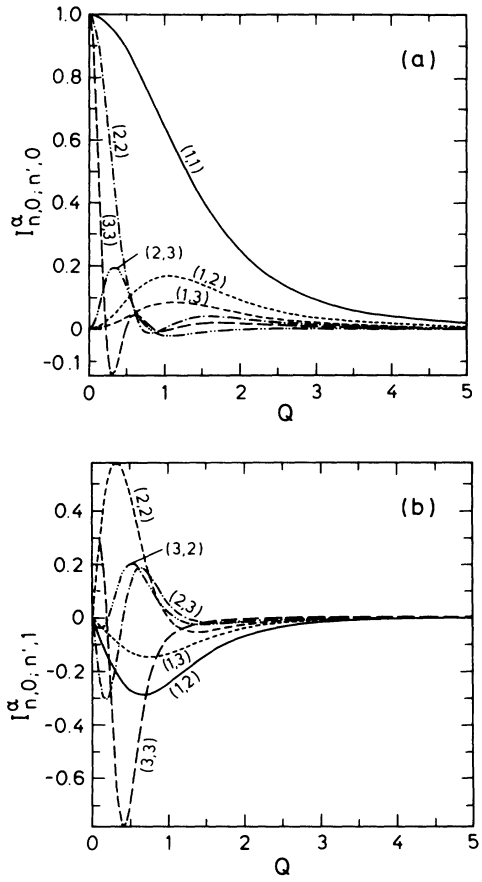


FIG. 2. Matrix elements $I_{n,0;n',l'}$ as a function of the dimensionless variable $Q$ for different values of $n$ and $n'$ (from 1 to 3) with angular momentum (a) $l' = 0$; (b) $l' = 1$. The numbers in brackets correspond to $(n, n')$.

$$C_{n,l';k,l} = (-1)^{l'+1}\frac{2^{l+2}k^{l+1}e^{\pi/2k}|\Gamma(l+1+i/k)|}{(2l+1)!n^{l'+2}} \times\sqrt{\frac{(n+l')!}{(n-l'-1)!}} \tag{28}$$

and $\mathcal{I}_{n,0;k,l}(Q)$ is given by Eq. (B11) of Appendix B. Similar formulas can be obtained for the matrix elements between $\{n,0\}$ and $\{k,l\}$ states. The following relation is fullfilled:

$$I_{k,l;n,0}(Q) = I_{n,0;-k,l}(Q). \tag{29}$$

No simple relationship can be obtained between $I_{n,0;k,l}(Q)$ and $I_{n,l;k,0}(Q)$. The matrix elements corresponding to $\{n,l\}$ and $\{k,0\}$ transitions can be written as

$$I_{n,l;k,0}(Q) = C_{n,l;k,0}\sqrt{\frac{a^3}{V}}Q^l\left(\frac{d}{QdQ}\right)^l \times\left\{\frac{1}{2iQ}(\mathcal{I}_{n,l;k,0}(Q) - \mathcal{I}_{n,l;k,0}(-Q))\right\} , \tag{30}$$

where now

$$\mathcal{I}_{n,l;k,0}(Q) = \sum_{s=0}^{n-l-1} \frac{(l+1-n)_s}{(2l+2)_s} \frac{2^s}{n^s}(s+1)\frac{(1/n+ik-iQ)^{s+2}}{[(1/n+ik)^2+Q^2]^{s+2}} F\left(i/k+1, s+2, 2l'+2; \frac{2ik}{1/n+ik+iQ}\right) . \quad (31)$$

Because the function $\varphi_{k,l,0}(\mathbf{r})$ is real the following relations hold:

$$I_{n,l;k,0}(Q) = (-1)^l I_{k,0;n,l}(Q),$$
$$I_{n,l;k,0}(Q) = (-1)^l I_{n,l;k,0}(-Q) . \quad (32)$$

We have plotted in Fig. 3 the matrix elements $I_{n,0;k,0}(Q)$ in units of $\sqrt{a^3/V}$ as a function of the variables $k$ and $Q$ for $n = 1$–3. For $n = 1$ [Fig. 3(a)] the maximum contribution is in the region $0 < Q < 2$; $0 < k < 3$, while when $n$ increases the integration area in $k$ and $Q$ rapidly decreases. As will be seen below [Eq. (39)] the contribution of the discrete-continuous matrix elements to the scattering amplitude can be limited to a few values of the principal quantum number $n$.

For the continuous-continuous transitions and using the wave function (22) it is clear that

$$I_{\mathbf{k},\mathbf{k}'}(\mathbf{Q}) = (2\pi)^3 \frac{a^3}{V}\delta(\mathbf{k}' - \mathbf{k} + \mathbf{Q}) . \quad (33)$$

## III. RAMAN TENSOR

According to Eqs. (14) and (15) and for isotropic masses the Raman tensor for the impurity-induced LO-phonon Fröhlich interaction is diagonal, i.e.,

$$\overleftrightarrow{\mathrm{R}}_i = \begin{pmatrix} \mathsf{a}_i(q) & 0 & 0 \\ 0 & \mathsf{a}_i(q) & 0 \\ 0 & 0 & \mathsf{a}_i(q) \end{pmatrix} . \quad (34)$$

For a given impurity concentration equal to $n_i$, the total squared Raman polarizability $\hat{\mathbf{e}}_l \parallel \hat{\mathbf{e}}_s$

$$|\mathsf{a}_{Fi}|^2 = n_i V \sum_{\mathbf{q}} |\mathbf{e}_l \cdot \overleftrightarrow{\mathrm{R}}(\mathbf{q}) \cdot \mathbf{e}_s|^2 \quad (35)$$

can be obtained by writing $\mathsf{a}_i$ as a function of the amplitude probability and introducing the above calculated matrix elements into Eq. (15); then

$$|\mathsf{a}_{Fi}|^2 = S_0 \int_0^\infty dx\, g^2(x) |\sum_{j=1}^{4} F_j(x)|^2 , \quad (36)$$

where

$$S_0 = \frac{V V_c n_i a}{\pi^2}\left[\frac{2\sqrt{2\hbar\omega_0 R_H}}{\hbar\omega_l\sqrt{\hbar\omega_l\hbar\omega_s}}\frac{|C_F|}{\varepsilon_0} a_H \left(\frac{a_H}{a}\right)^2\left(\frac{R_H}{R}\right)^2 \times\sqrt{\frac{M}{m}}\frac{2}{3}\frac{P^2}{mR}\right]^2 , \quad (37)$$

$a_H$ and $R_H$ being the hydrogen Bohr radius and Rydberg, respectively, and $P$ the oscillator strength of the transition ($P = |\langle s|p_x|x\rangle|$). The $S_0$ parameter has units of length to the fourth, in this way the functions in the integrand in Eq. (36) are dimensionless. The terms $F_i$ ($i = 1,2,3,4$) in Eq. (36) correspond to different virtual exciton states: in $F_1(x)$ all intermediate states belong to the discrete spectrum,

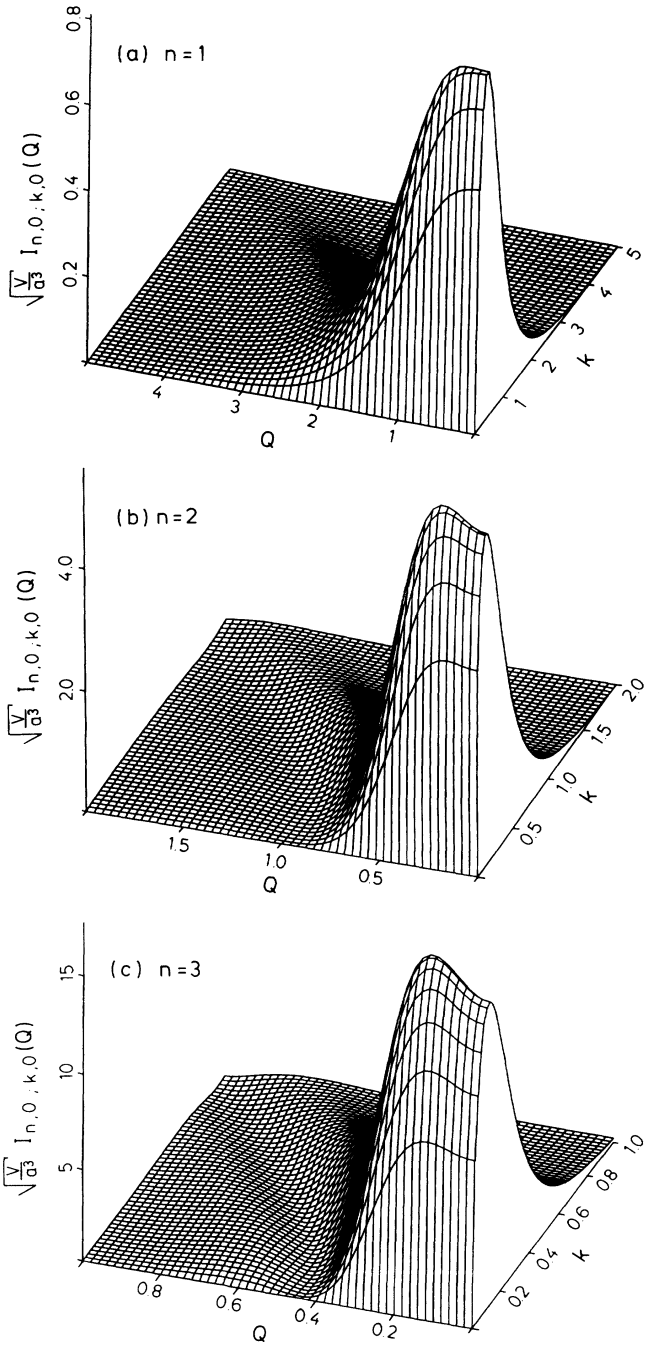


FIG. 3. Matrix elements $I_{n,0;k,0}\sqrt{V/a^3}$ as a function of the dimensionless variables $k$ and $Q$ for several values of $n$, (a) $n = 1$, (b) $n = 2$, (c) $n = 3$.

$$F_1(x) = \sum_{n,n',n''=1}^{\infty} \sum_{l'=1}^{n'-1} \frac{1}{(nn'')^{3/2}} \frac{(-1)^{l'} I^h_{n,0;n',l'}(x) - I^e_{n,0;n',l'}(x)}{(\beta_1 + 1/n^2)(\beta_3 + 1/n''^2)} [(-1)^{l'} I^h_{n'',0;n',l'}(x) - I^e_{n'',0;n',l'}(x)]$$
$$\times \left( \frac{1}{\beta_2 - \hbar\omega_0/R + 1/n'^2} + \frac{1}{\beta_2 + 1/n'^2} \right) . \tag{38}$$

In $F_2(x)$ two intermediate states belong to the discrete spectrum and one to the continuum. In this case different transitions can be performed: (a) discrete-discrete-continuous, (b) continuous-discrete-discrete, (c) discrete-continous-discrete. For example, in case (a) the light creates an exciton in the virtual state $|n, l = 0, m = 0\rangle$ (discrete state) by the emission of one phonon [diagram (b) in Fig. 1], the exciton made the transition from $|n, l = 0, m = 0\rangle$ to another discrete state with quantum numbers $|n', l', m = 0\rangle$, the scattering by impurities moves the exciton from $|n', l', m = 0\rangle$ to $|k, l'' = 0, m = 0\rangle$ state (continuous state) from where the exciton annihilation is produced with an emission of a quantum of light. Considering all these possibilities the function $F_2(x)$ is

$$F_2(x) = \frac{1}{2\pi} \sqrt{\frac{V}{a^3}} \sum_{n=1}^{\infty} \frac{1}{n^3} \left[ \sum_{n'=1}^{\infty} \sum_{l'=1}^{n'-1} [(-1)^{l'} I^h_{n,0;n',l'}(x) - I^e_{n,0;n',l'}(x)] \right.$$
$$\times \left( \frac{1}{\beta_2 - \hbar\omega_{\rm LO}/R + 1/n'^2} + \frac{1}{\beta_2 + 1/n'^2} \right)$$
$$\times \int_0^{\infty} dk\, k [I^h_{n',l';k,0}(x) - I^e_{n',l';k,0}(-x)] e^{\pi/2k} |\Gamma(1 - i/k)|$$
$$\times \left( \frac{1}{(\beta_1 + 1/n^2)(\beta_3 - k^2)} + \frac{1}{(\beta_1 - k^2)(\beta_3 + 1/n^2)} \right)$$
$$+ \sqrt{\frac{V}{a^3}} \sum_{n''=1}^{\infty} \frac{1}{n''^{3/2}} \sum_{l=0}^{n''-1} \int_0^{\infty} \frac{I^h_{n,0;k,l}(-x) - I^e_{n,0;k,l}(x)}{\beta_1 + 1/n^2} k\, dk$$
$$\times \frac{I^h_{k,l;n'',0}(x) - I^e_{k,l;n'',0}(-x)}{\beta_3 + 1/n''^2}$$
$$\left. \times \left( \frac{1}{\beta_2 - \hbar\omega_{\rm LO}/R - k^2} + \frac{1}{\beta_2 - k^2} \right) \right] . \tag{39}$$

The contribution due to two continuous exciton states and one discrete virtual state is given through the function $F_3(x)$ where all combinations have been taken into account (discrete-continuous-continuous plus continuous-continuous-discrete plus continous-discrete-continuous transitions). It is possible to show that $F_3(x)$ can be put in the form

$$F_3(x) = \frac{1}{4\pi} \sqrt{\frac{V}{a^3}} \left\{ \sum_{n=1}^{\infty} \frac{1}{n^{3/2}} \sum_{l=0}^{n-1} \int_0^{\infty} dk\, e^{\pi/2k} |\Gamma(1 - i/k)| [I^h_{n,0;k,l}(-x) - I^e_{n,0;k,l}(x)] \right.$$
$$\times \left( \frac{1}{(\beta_1 + 1/n^2)(\beta_3 - k^2)} + \frac{1}{(\beta_1 - k^2)(\beta_3 + 1/n^2)} \right)$$
$$\times \left[ \frac{1}{2xm_h/m_E} ln \left( \frac{\beta_2 - \hbar\omega_{\rm LO}/R - (k - xm_h/m_E)^2}{\beta_2 - \hbar\omega_{\rm LO}/R - (k + xm_h/m_E)^2} \frac{\beta_2 - (k - xm_h/m_E)^2}{\beta_2 - (k + xm_h/m_E)^2} \right) \right.$$
$$\left. - \frac{1}{2xm_e/m_E} ln \left( \frac{\beta_2 - \hbar\omega_{\rm LO}/R - (k - xm_e/m_E)^2}{\beta_2 - \hbar\omega_{\rm LO}/R - (k + xm_e/m_E)^2} \frac{\beta_2 - (k - xm_e/m_E)^2}{\beta_2 - (k + xm_e/m_E)^2} \right) \right]$$
$$+ \frac{2}{\pi} \sqrt{\frac{V}{a^3}} \sum_{n=1}^{\infty} \sum_{l=0}^{n-1} \int_0^{\infty} dk\, k \frac{e^{\pi/2k} |\Gamma(1 - i/k)|}{(\beta_1 - k^2)} [I^h_{k,0;n,l}(-x) - I^e_{k,0;n,l}(x)]$$
$$\times \int_0^{\infty} dk\, k \frac{e^{\pi/2k} |\Gamma(1 - i/k)|}{(\beta_3 - k^2)} [I^h_{k,0;n,l}(-x) - I^e_{k,0;n,l}(x)]$$
$$\left. \times \left( \frac{1}{\beta_2 - \hbar\omega_{\rm LO}/R + 1/n^2} + \frac{1}{\beta_2 + 1/n^2} \right) \right\} . \tag{40}$$

The term $F_4(x)$ corresponds to the contribution of only continuous virtual states to the scattering efficiency, and can be written as

$$F_4(x) = \frac{1}{2(2\pi)^2} \int d^3k \int d^3k' \int d^3k'' \frac{\delta(\mathbf{k}-\mathbf{k}'+xm_h/m_E) - \delta(\mathbf{k}-\mathbf{k}'-xm_e/m_E)}{\beta_1 - k^2} \times \frac{\delta(\mathbf{k}-\mathbf{k}''-xm_h/m_E) - \delta(\mathbf{k}-\mathbf{k}''+xm_e/m_E)}{\beta_3 - k''^2} \times \left( \frac{1}{\beta_2 - \hbar\omega_{\mathrm{LO}}/R - k'^2} + \frac{1}{\beta_2 - k'^2} \right). \quad (41)$$

The functions $\beta_i$ $(i = 1, 2, 3)$ are defined as follows:

$$\beta_1 = \frac{\hbar\omega_l - E_g + i\Gamma_1}{R},$$
$$\beta_2 = \frac{\hbar\omega_l - E_g + i\Gamma_2}{R} - \frac{\mu}{m_E}x^2, \quad (42)$$
$$\beta_3 = \frac{\hbar\omega_s - E_g + i\Gamma_3}{R}.$$

In Fig. 4(a) squared magnitudes of the different contributions

$$\frac{|a_j|^2}{S_0} = \int_0^\infty dx\, \bar{g}^2(x)|F_j(x)|^2 \quad (j = 1, 2, 3, 4) \quad (43)$$

for the case of scattering by ionized impurities, i.e., for $\bar{g} = [x^2 + (a/\lambda)^2]^{-1}$, are presented as a function of the reduced laser photon energy $(\hbar\omega_l - E_g)/R$ for the case $\hbar\omega_{\mathrm{LO}}/R = 4.55$ and $a/\lambda = 0.186$. The total squared Raman polarizability $|a_{Fi}|^2/S_0$ is also shown. The following empirical relation is used for the lifetime broadenings:[16]

$$\Gamma_n = \Gamma(k) - \frac{\Gamma(k) - \Gamma_1}{n^2} \quad (44)$$

with $\Gamma(k) = 10$ meV and $\Gamma_1 = 5$ meV. The most important contribution to the Raman tensor comes from the function $a_1$ (involving discrete-discrete-discrete exciton states) and gives, for these particular data, an incoming resonance larger than the outgoing one. All other terms give outgoing resonances stronger than incoming ones. This is due to the possibility of triple resonance introduced by the continuum in the outgoing resonance for a particular value of $Q$.

Figure 4(b) shows the squared Raman polarizability $|a_{Fi}|^2$ in units of $S_0$ including the excitonic effect (solid line) and the corresponding calculation for the uncorrelated $|a^u_{Fi}|^2$ electron-hole pair theory[3] (dashed line) as a function of the reduced laser photon energy $(\hbar\omega_l - E_g)/R$. As can be seen in Fig. 4(b) $|a^u_{Fi}|^2$ is two orders of magnitude lower than the $|a_{Fi}|^2$ calculated according to the impurity-exciton theory.

### A. Broadening and screening effects

Figure 5 displays the results of the calculation of $|a_{Fi}|^2$ with Eq. (36) obtained for the GaAs with the parameters of the $E_0 + \Delta_0$ gap[18] for three different values of the $1s$-exciton broadening $\Gamma_{1s}$ (5, 10, and 14 meV).[30] In all calculations a continuous exciton broadening $\Gamma_c = 14$

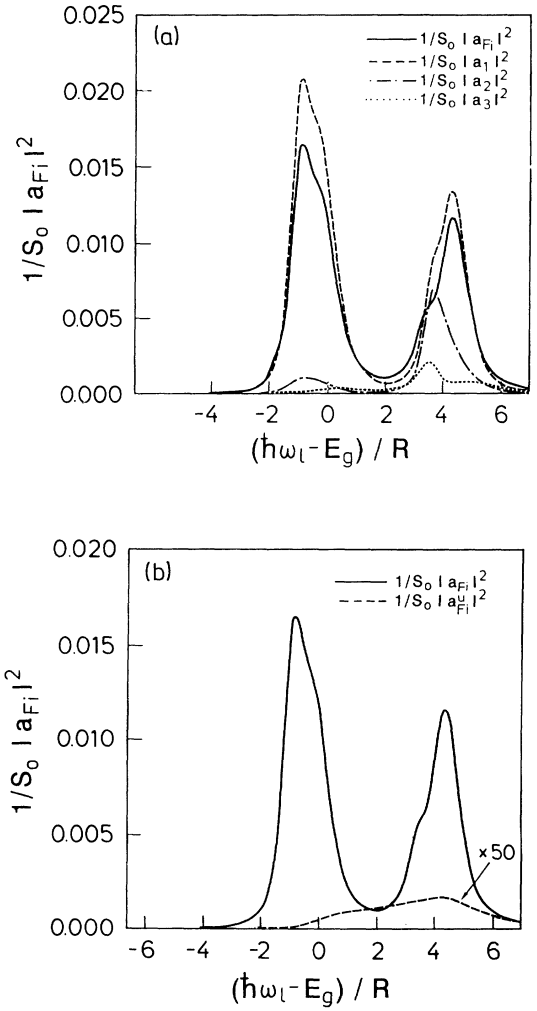


FIG. 4. (a) The different contributions, $\frac{1}{S_0}|a_j|^2$ $(j = 1, 2, 3, 4)$, to the Raman efficiency calculated for the extrinsic impurity-induced forbidden scattering by one LO phonon as a function of incident photon energy in dimensionless units are shown together with the total Raman efficiency $|a_{Fi}|^2/S_0$. $j = 1$, all three intermediate states belong to the discrete spectrum; $j = 2$, two intermediate states belong to the discrete and one to the continuum; $j = 3$, two intermediate states belong to the continuum and one to the discrete spectrum. (b) Impurity induced LO-phonon Raman efficiency. Solid line: excitonic theory given by Eq. (36) in units of $S_0$. Dashed line: uncorrelated electron-hole theory $|a^u_{Fi}|^2$ according to Ref. 3. The curve $|a^u_{Fi}|^2/S_0$ has been multiplied by a factor of 50. In the calculation the GaP parameters were used (Ref. 17) and the ionized impurity is assumed with a screening factor $\lambda = 5.4a$.

meV was taken and a concentration of ionized donors $n_i = 10^{14}$ and $10^{17}$ cm$^{-3}$ were assumed. Using the Thomas-Fermi model for the screening factor, values of $a/\lambda = 0.17$ and 1.7 are obtained for these impurity concentrations. Figure 5 shows that the incoming resonance is always stronger than the outgoing one for $a/\lambda = 0.17$. However, the intensity ratio of both peaks decreases when the importance of discrete transitions is reduced (i.e., when $\Gamma_{15}$ increases). They are of the same order when $\Gamma_{15} = \Gamma_c = 14$ meV. When the impurity concentration is high, $a/\lambda = 1.7$, Fig. 5(b) shows that screening favors the continuous transitions and for $\Gamma_{15} = 10$ and 14 meV the outgoing peak is stronger than the incoming one. This difference is due to the $\mathbf{q}$ dependence on the functions $F_j(\mathbf{q})$ ($j$ = 1,2,3,4) in Eq. (36). Under incoming resonance condition ($\hbar\omega_l \simeq E_g - R$) the most important contribution to the scattering intensity comes from small $\mathbf{q}$ values, while for the outgoing resonance ($\hbar\omega_l \simeq E_g - R + \hbar\omega_{LO}$) phonons with large $\mathbf{q}$ vectors are favored. Thus, the Raman intensity should be less sensitive to the values of $\lambda$ for outgoing resonance while for incoming resonance the intensity decreases more drastically with decreasing values of $\lambda$.

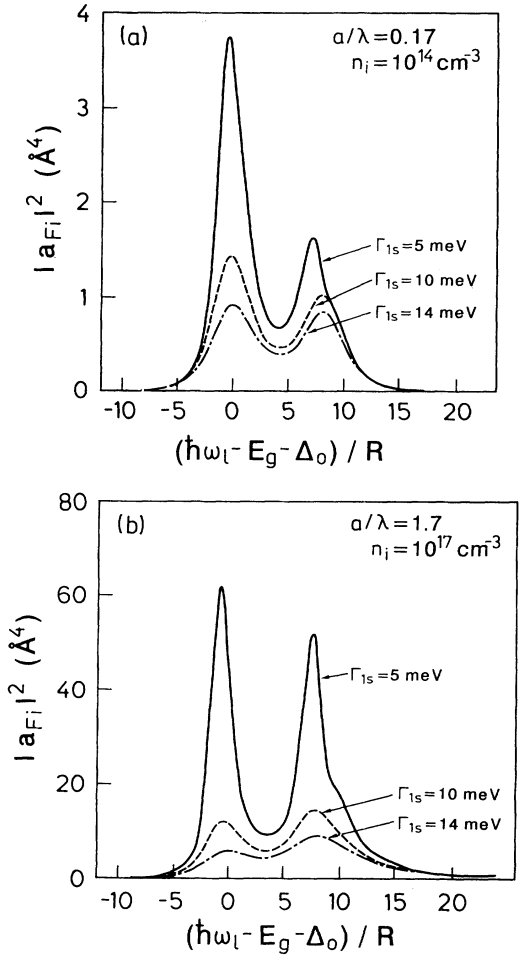


FIG. 5. Raman efficiency for extrinsic impurity-induced LO-Fröhlich scattering calculated with Eq. (36) using the parameters appropiate to GaAs in the $E_0 + \Delta_0$ critical point (Ref. 17) for three different values of $\Gamma_{1s} = 5, 10$, and 14 meV and $\Gamma_c = 14$ meV. (a) Screening parameter $a/\lambda = 0.17$ for $n_i = 10^{15}$ cm$^{-3}$, and (b) $a/\lambda = 1.7$ for $n_i = 10^{17}$ cm$^{-3}$.

### B. Ionized impurities versus neutral impurities

The only difference between these two scattering mechanisms arises from the impurity vertex $g(\mathbf{q})$ in the calculation of the Raman efficiency. For ionized impurities this function is written as (see Appendix A)

$$g(\mathbf{q}) = \frac{4\pi e^2}{\varepsilon_0 V_0} \frac{1}{q^2 + \lambda^{-2}} \cdot \tag{45}$$

The simplest way to estimate $\lambda$ is the Thomas-Fermi model which yields $\lambda = (3\pi^2 n_i)^{-1/3}$. Nevertheless, other models can be used to describe more precisely the screening effects.[31] For neutral impurities, Eq. (42) must be replaced by

$$g(\mathbf{q}) = \frac{4\pi e^2}{\varepsilon_0 V_0} \frac{1}{q^2 + 4/a_i^2} \left(1 + \frac{4/a_i^2}{(q^2 + 4/a_i^2)^2}\right) \cdot \tag{46}$$

By comparing Eqs. (45) and (46) it becomes clear that both mechanisms lead to the same behavior when the impurity Bohr radius $a_i \sim 2\lambda$. The final results for $|\mathbf{a}_{Fi}|^2$ obtained from both impurity scattering mechanisms for the GaAs parameters of the $E_0 + \Delta_0$ CP are plotted in Fig. 6. The solid line represents the scattering intensity induced by ionized impurities for $\lambda = a$. The other curves correspond to the neutral impurity mechanism for different ratios of $a_i/a$ (2,1,0.5). The neutral impurities with a Bohr radius small in comparison with that of the exciton give a negligible contribution to the scattering efficiency.

### C. Fröhlich interaction versus impurity-induced LO Raman scattering

In backscattering configuration on the (001) surface the Raman efficiency in the $z(x,x)\bar{z}$ geometry amounts to

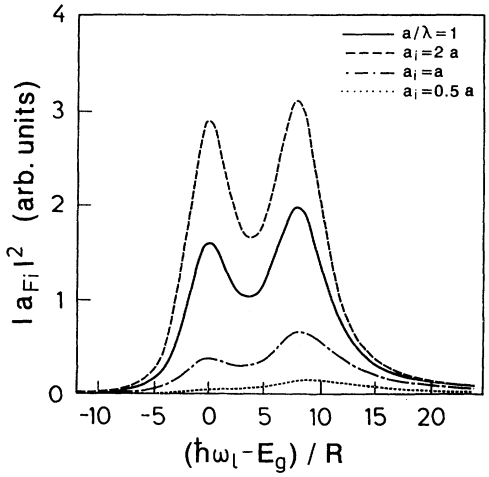


FIG. 6. Raman efficiency for extrinsic impurity-induced forbidden scattering by one LO phonon. Solid line: ionized impurity with $\lambda = a$. The other curves are calculated according to Eqs. (36) and (46) (neutral impurities) for several values of the ration $a_i/a$ (0.5, 1, 2). The GaAs data were used with $\Gamma_{1s} = \Gamma_c = 14$ meV.

$$|a|^2 = |a_F|^2 + |a_{Fi}|^2 \ , \tag{47}$$

where $a_F$ represents the Raman polarizability for wave-vector-induced Fröhlich interaction. The diagonal components $a_F$ of the Raman tensor for the case of transitions between exciton states is given in Ref. 17. An analysis of the different contributions to the squared Raman polarizability shows that the outgoing resonance in the squared Raman polarizability $|a_F|^2$ is higher than the incoming one because of the contribution of discrete-continuous excitonic transitions. It is well known that the scattering amplitude for the Fröhlich mechanism is proportional to the magnitude phonon wave vector $\mathbf{q}$ which is equal to $\kappa_l - \kappa_s$ since in this case the wave vector is conserved. For impurity-induced Fröhlich interaction the phonon vector $\mathbf{q}$ is not limited to any particular value. The main contributions to the Raman scattering efficiency come from $\mathbf{q}$ near the values $\mathbf{q}_1$ and $\mathbf{q}_2$ determined by the relations

$$\hbar\omega_l - E_\beta - \frac{\hbar^2 q_1^2}{2m_E} = 0 \tag{48a}$$

and

$$\hbar\omega_l - \hbar\omega_{\mathrm{LO}} - E_\beta - \frac{\hbar^2 q_2^2}{2m_E} = 0. \tag{48b}$$

The $\mathbf{q} = \mathbf{q}_1$ or $\mathbf{q} = \mathbf{q}_2$ values correspond to real exciton transitions for the intermediate state $\beta$ in Figs. 1(a) and 1(b), respectively. These real transitions are determined by the zeros in the corresponding denominators of Eq. (15) and produce double and triple resonance effects. Equation (48a) is the double resonance condition while Eq. (48b) represents triple resonance. The latter explains why the Raman scattering efficiency for the outgoing resonance is higher than for the incoming resonance.

In Fig. 7 we compare the absolute value of the Fröhlich interaction $|a_F|^2$, calculated including excitonic effects (see Ref. 17) and impurity-induced $|a_{Fi}|^2$ for the $E_0+\Delta_0$ CP of GaAs with different impurity concentrations. Note that we need a value of $n_i = 10^{18}$ cm$^{-3}$ in order to have $|a_{Fi}|^2$ of the same order as the $q$-induced $|a_F|^2$. This small contribution is explained by the $(q^2+1/\lambda^2)^{-2}$ factor present in Eq. (36), which drastically reduces the main contribution of large $\mathbf{q}$ vectors to the Raman efficiency. For these calculations $\lambda^{-1} = 0$ and $\Gamma_{1s} = \Gamma_c = 14$ meV were taken. From this comparison we conclude that in high-purity liquid-phase epitaxy samples the only contribution to the Raman polarizability in the $\bar{z}(x,x)z$ configuration comes from Fröhlich interactions, as was already pointed out in Ref. 18. The experimental data for GaAs measured at 100 K obtained from Ref. 5 are also presented in Fig. 7. It is clearly seen that dipole-forbidden Fröhlich interaction fits the experiment without assuming the impurity-induced mechanism.

Figure 8 shows the calculated absolute value of the squared Raman polarizability for AlSb around the $E_0$ CP. The forbidden Fröhlich $|a_F|^2$ and the total absolute value $|a_F|^2 + |a_{Fi}|^2$ with $n_i = 2 \times 10^{18}$ cm$^{-3}$ are presented together with experimental points.[22] The parameters used for AlSb are those of Ref. 22 and $\lambda^{-1} = 0$ was used. The order of magnitude of $|a_{Fi}|^2$ obtained in Ref. 22 treating the contribution of impurities to the Fröhlich mechanism in a simple, heuristic way is reproduced in Fig. 8 adding $a_{Fi}$ in a rigorous way according to Eq. (36). The samples used in Ref. 22 are $p$-type commercial samples with impurity concentrations higher than $10^{17}$ cm$^{-3}$. It is thus possible that impurities play an important role in the measurements reported for AlSb. This should be clarified by simultaneous Raman and Hall effect measurements for the same samples. We note, however that the width of the experimental profile in Fig. 8 is much larger than the calculated one. In view of the sensitivity of AlSb surfaces to humidity and the delicate polishing procedure required, the measurements should be repeated, prefer-

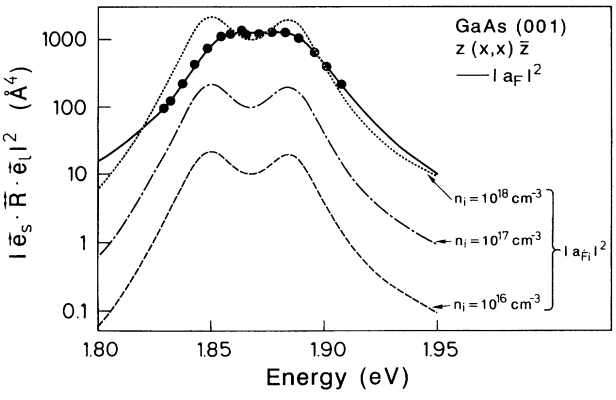


FIG. 7. Raman polarizability calculated for forbidden LO-phonon scattering in GaAs around the $E_0 + \Delta_0$ gap. Solid line: intrinsic LO-phonon Raman scattering $|a_F|^2$ (see Ref. 17) including excitonic effects. The other curves represent the calculated $|a_{Fi}|^2$ [see Eq. (36)] for $n_i = 10^{16}, 10^{17}$, and $10^{18}$ cm$^{-3}$. Parameters from Ref. 18, $\lambda^{-1} = 0$, and $\Gamma_{1s} = \Gamma_c = 14$ meV. The dots are experimental points after Ref. 5.

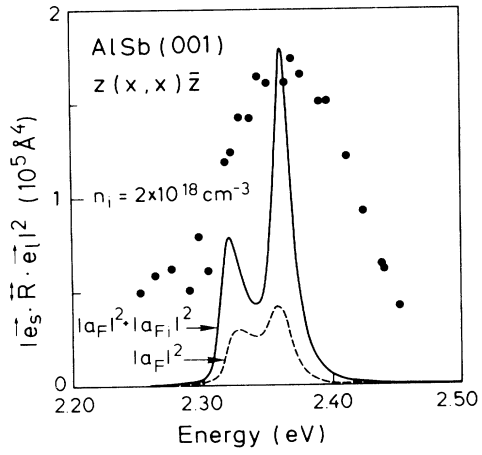


FIG. 8. Forbidden LO-phonon Raman polarizability for AlSb at the $E_0$ gap. Solid line: total absolute value of $|a_F|^2 + |a_{Fi}|^2$ for LO-phonon Raman scattering including excitonic effects. Dashed line: $|a_F|^2$ for intraband Fröhlich LO-phonon Raman scattering (see Ref. 17). Parameters from Ref. 22. The dots are experimental points after Ref. 22.

ably for surfaces cleaved in vacuum.

We should point out that the Raman efficiency is connected with the exciton lifetime broadening $\Gamma = \hbar/\tau$ and this is related to the relaxation time $\tau_I$ due to the impurity scattering. In general we can write that

$$\frac{1}{\tau} = \frac{1}{\tau_I} + \frac{1}{\tau_0} , \tag{49}$$

where $\tau_0$ is the relaxation time due to other scattering mechanisms like acoustic and optic phonon scattering. $1/\tau_I$ is proportional to the impurity concentration according to the relation[32]

$$\frac{1}{\tau_I} = \frac{2n_i\hbar^2}{m_E}\sqrt{\frac{2\pi}{m_E k_B T}}[1 - \alpha e^{\alpha} E_i(-\alpha)], \tag{50}$$

where $E_i$ is the integral exponential function,[28] $\alpha = \epsilon_i/k_B T$, and $\epsilon_i$ the binding energy. An estimation of $\Gamma_I = 1/\tau_I$ for the GaAs parameters, $T = 100$ K and $n_i = 10^{17}$ cm$^{-3}$ gives $\Gamma_1 \sim 3$ meV. For higher values of $n_i$, impurity scattering dominates and maximum Raman polarizability should rapidly decrease.

## IV. CONCLUSIONS

We have developed a theoretical model of impurity-induced first-order resonant Raman scattering which includes excitons as intermediate states in the Raman process. The obtained results confirm that the most important contribution to the forbidden one-phonon Raman process comes from the $q$-dependent Fröhlich interaction induced Raman scattering $|a_F|^2$. The impurity scattering mechanism becomes important for relatively high impurity concentrations ($\sim 10^{18}$ cm$^{-3}$). Neutral impurity scattering is important in the one LO-phonon Raman scattering for values of impurity radius of the order of the exciton Bohr radius. The calculated absolute values of $|a_F|^2 + |a_{Fi}|^2$ reproduce, for instance, the order of magnitude observed in AlSb for $T = 100$ K with $n_i = 2\times 10^{18}$ cm$^{-3}$.

## APPENDIX A: EXCITON-IMPURITY INTERACTION HAMILTONIAN

For ionized impurities and considering the screening effect, the electron-impurity potential interaction is equal to

$$U_e(\mathbf{r}_e) = \frac{e^2}{\varepsilon_0 r_e} e^{-r_e/\lambda} , \tag{A1}$$

where $\lambda$ is the screening length and $\mathbf{r}_e$ the electron coordinate. In the $\mathbf{q}$ representation Eq. (A1) can be written as

$$U_e(\mathbf{r}_e) = \sum_{\mathbf{q}} g_e(\mathbf{q}) e^{i\mathbf{q}\cdot\mathbf{r}_e} \tag{A2}$$

with

$$g_e(\mathbf{q}) = \frac{e^2}{\varepsilon_0 V}\int \frac{d^3 r_e}{r_e} e^{-i\mathbf{q}\cdot\mathbf{r} - r_e/\lambda} = \frac{4\pi e^2}{\varepsilon V}[q^2 + (1/\lambda)^2]^{-1} \tag{A3}$$

and for the hole $g_e(\mathbf{q}) = -g_h(\mathbf{q}) = g(\mathbf{q})$ with $\mathbf{r}_e$ replaced by the hole coordinate $\mathbf{r}_h$. Thus, the electron-hole-impurity potential is

$$U(\mathbf{r}_e, \mathbf{r}_h) = U_e(\mathbf{r}_e) + U_h(\mathbf{r}_h) . \tag{A4}$$

In the $\mathbf{K}, \lambda$-exciton representation and using second quantization the above equation is transformed into

$$H_{\text{exc-}i} = \sum_{\mathbf{K}',\lambda'}\sum_{\mathbf{K},\lambda}\frac{1}{V}\left(\int e^{-i\mathbf{K}'\cdot\mathbf{R}}\varphi^*_{\lambda'}(\mathbf{r})U(\mathbf{R},\mathbf{r})e^{i\mathbf{K}\cdot\mathbf{R}} \times\varphi_{\lambda}(\mathbf{r})d^3R\,d^3r\right) d^{\dagger}_{\lambda',\mathbf{K}'}d_{\lambda,\mathbf{K}} \tag{A5}$$

with

$$\mathbf{r} = \mathbf{r}_e - \mathbf{r}_h, \quad \mathbf{R} = \frac{m_e}{m_E}\mathbf{r}_e + \frac{m_h}{m_E}\mathbf{r}_h . \tag{A6}$$

From Eqs. (A2)–(A5) follows the exciton-impurity Hamiltonian of Eq. (11).

The neutral impurities can be treated in the hydrogenic approximation; the electrostatic potential is the solution of the Poisson equation

$$\nabla^2\phi = -\frac{4\pi}{\varepsilon_0} e|\psi_n(\mathbf{r})|^2 , \tag{A7}$$

where $\psi_n(\mathbf{r})$ is the impurity wave function. For the $1s$ state the corresponding density of charge is given by

$$\rho(\mathbf{r}) = -\frac{e}{\pi a_i^3} e^{-2r/a_i}, \tag{A8}$$

$a_i$ being the impurity Bohr radius. Combining (A8) with (A7) and adding the boundary condition for $\phi(\mathbf{r})$ in $r \to \infty$ and $r \to 0$, the full solution for the electron-impurity potential interaction $U_e(\mathbf{r}_e) = e\phi(\mathbf{r}_e)$ is given by

$$U_e(\mathbf{r}_e) = \frac{e^2}{\varepsilon_0 r} e^{-2r/a_i}\left(\frac{r}{a_i} + 1\right) . \tag{A9}$$

Following the same procedure as in the ionized-impurity case the exciton-neutral impurity Hamiltonian is obtained now with $g(\mathbf{q})$ equal to

$$g(\mathbf{q}) = \frac{4\pi e^2}{\varepsilon_0 V}\frac{1}{q^2 + 4/a_i^2}\left(1 + \frac{4/a_i^2}{(q^2 + 4/a_i^2)^2}\right) . \tag{A10}$$

## APPENDIX B: MATRIX ELEMENTS

According to Eq. (16) it is necessary to evaluate the transition between $\varphi_{n,0,0}$ and $\varphi_{n',l',0}$ exciton states. The discrete-discrete matrix elements $I_{n,0;n',l'}(Q)$ are obtained by substituting Eq. (18) into Eq. (10), i.e.,

$$I_{n,0;n',l'}(Q) = a^3 \int d^3\rho\, \varphi^*_{n,0,0}(\boldsymbol{\rho}) e^{i\mathbf{Q}\cdot\boldsymbol{\rho}} \varphi_{n',l',0}(\boldsymbol{\rho})$$
$$= \frac{i^{l'} 2^{l'+1}}{(2l'+1)! n^{3/2} n'^{l'+2}} \sqrt{\frac{(2l'+1)(n'+l')!}{(n'-l'-1)!}}$$
$$\times \int_0^\infty d\rho\, \rho^{l'+2} e^{-\rho(1/n+1/n')} F\left(-n+1, 2; \frac{2\rho}{n}\right) F\left(-n'+l'+1, 2l'+2; \frac{2\rho}{n}\right)$$
$$\times \int_{-1}^{1} dx P_{l'}(x) e^{iQ\rho x}\ , \tag{B1}$$

where $P_l(x)$ are the Legendre polynomials, $\boldsymbol{\rho} = \mathbf{r}/a$, and the $\mathbf{Q}$ vector has been taken along the $z$ axis. The integral in $x$ yields[27]

$$\int_{-1}^{1} dx\, P_{l'}(x) e^{iQ\rho x} = \sqrt{\frac{2\pi}{Q\rho}} i^{l'} J_{l'+1/2}(Q\rho), \tag{B2}$$

where $J_{l'+1/2}(Q\rho)$ is a Bessel function of order $l' + \frac{1}{2}$. The function $J_{l'+1/2}(Q\rho)$ can be represented by[29]

$$J_{l'+1/2}(Q\rho) = (-1)^{l'} \sqrt{\frac{2Q\rho}{\pi}} \frac{Q^{l'}}{\rho^{l'+1}} \left(\frac{\partial}{Q\partial Q}\right)^{l'} \left(\frac{\sin Q\rho}{Q\rho}\right). \tag{B3}$$

Applying (B2) and (B3) to Eq. (B1),

$$I_{n,0;n',l'}(Q) = -C_{n,0;n',l'} Q^{l'} \left(\frac{d}{QdQ}\right)^{l'} \left[\frac{1}{2iQ} \int_0^\infty d\rho\, \rho e^{-\rho(1/n+1/n')} \left(e^{iQ\rho} - e^{-iQ\rho}\right)\right.$$
$$\left. \times F\left(-n+1, 2; \frac{2\rho}{n}\right) F\left(-n'+l'+1, 2l'+2, \frac{2\rho}{n'}\right)\right], \tag{B4}$$

where

$$C_{n,0;n',l'} = \frac{-2^{l'+2}}{(2l'+1)! n^{3/2} n'^{l'+2}} \sqrt{\frac{(2l'+1)(n'+l')!}{(n'-l'-1)!}}. \tag{B5}$$

The integral

$$\mathcal{I}_{n,0;n',l'}(Q) = \int_0^\infty d\rho\, \rho e^{-\rho(1/n+1/n'+iQ)}$$
$$\times F\left(-n+1, 2; \frac{2\rho}{n}\right)$$
$$\times F\left(-n'+l'+1, 2l'+2, \frac{2\rho}{n'}\right) \tag{B6}$$

can be solved by writing

$$F\left(-n+l+1, 2l+2; \frac{2\rho}{n}\right)$$
$$= \sum_{s=0}^{n-1-l} \frac{(1+l-n)_s}{(2l+2)_s (s+1)!} \frac{2^s}{n^s} \rho^s \tag{B7}$$

with $(1-m)_s = (1-m)(1-m+1)\cdots(s-m)$. The integral of an confluent hypergeometric function times a power is a normal hypergeometric function:[26,28]

$$\int_0^\infty e^{-\lambda z} z^\nu F(\alpha, \gamma; kz) dz$$
$$= \Gamma(\nu+1) \lambda^{-\nu-1} F\left(\alpha, \nu+1, \gamma; \frac{k}{\lambda}\right). \tag{B8}$$

In our case we have the $\Gamma$ function of an integer, $\Gamma(s+2) = (s+1)!$, and the solution of $\mathcal{I}_{n,0;n',l'}(Q)$ is

$$\mathcal{I}_{n,0;n',l'}(Q) = \sum_{s=0}^{n-1} \frac{(1-n)_s}{s! n^s} 2^s \frac{(1/n + 1/n' - iQ)^{s+2}}{[(1/n+1/n')^2 + Q^2]^{s+2}} F\left(-n'+l'+1, s+2, 2l'+2; \frac{2/n'}{1/n+1/n'+iQ}\right). \tag{B9}$$

The continuous-discrete matrix elements can be obtained by applying to Eq. (10) the wave functions given by Eqs. (18)

and (20). We obtain

$$I_{n,0;k,l}(Q) = \sqrt{\frac{a^3}{2\pi}} \frac{i^l 2^{l+2} k^{l+1} e^{\pi/2k} |\Gamma(l+1-i/k)|}{(2l+1)! n^{3/2}} \times \int_0^\infty d\rho\, \rho^{l+2} e^{-\rho(1/n+ik)} F(-n+1,2;2\rho/n) F(i/k+l+1,2l+2;2ik\rho) \int_{-1}^{1} dx\, P_l(x) e^{iQ\rho x}. \quad \text{(B10)}$$

According to Eqs. (B2) and (B3) and writing

$$\mathcal{I}_{n,0;k,l}(Q) = \int_0^\infty d\rho\, \rho e^{-\rho(1/n+ik+iQ)} F(i/k+l+1,2l+2;2ik\rho) F(-n+1,2;2\rho/n) = \sum_{s=0}^{n-1} \frac{(1-n)_s}{s! n^s} \frac{(1/n+ik-iQ)^{s+2}}{[(1/n+ik)^2+Q^2]^2} F\left(ik+l+1, s+2, 2l'+2; \frac{2ik}{1/n+ik+iQ}\right), \quad \text{(B11)}$$

the matrix element $I_{n,0;k,l}(Q)$ can be given in terms of $\mathcal{I}_{n,0;k,l}(Q)$, similarly to the discrete-discrete case and Eq. (25) is obtained straightforward. Following the same procedure the function $I_{n,l;k,0}(Q)$ can be calculated and Eq. (30) is derived.

---

*Permanent address: Department of Theoretical Physics, Havana University, Havana, Cuba.

†Permanent address: Departamento de Física Aplicada, Universidad de València, E-46100 València, Spain.

[1] M. Cardona, in *Light Scattering in Solids II*, edited by M. Cardona (Springer, Heidelberg, 1982), p. 19.

[2] W. Kauschke, V. Vorliček, and M. Cardona, Phys. Rev. B **36**, 9129 (1987).

[3] J. Menéndez and M. Cardona, Phys. Rev. B **31**, 3696 (1985).

[4] A. K. Sood, W. Kauschke, J. Menéndez, and M. Cardona, Phys. Rev. B **35**, 2886 (1987).

[5] W. Kauschke, M. Cardona, and E. Bauser, Phys. Rev. B **35**, 8030 (1987).

[6] J. Menéndez and M. Cardona, Phys. Rev. Lett. **51**, 1297 (1983).

[7] W. Kauschke and M. Cardona, Phys. Rev. B **33**, 5473 (1986).

[8] W. Kauschke and M. Cardona, Phys. Rev. B **35**, 9619 (1987).

[9] W. Limmer, H. Leiderer, K. Jakob, W. Gebhardt, W. Kauschke, A. Cantarero, and C. Trallero-Giner, Phys. Rev. B **42**, 11 325 (1990).

[10] C. Steineck, W. Limmer, H. H. Otto, and W. Gebhardt, J. Phys. C **21**, 3507 (1988).

[11] W. Limmer, H. Leiderer, K. Jakob, and W. Gebhardt, in *Proceedings of the 20th International Conference on the Physics of Semiconductors*, edited by E. M. Anastassakis and J. D. Joannopoulos (World Scientific, Singapore, 1990), p. 2005.

[12] W. Limmer, H. Leiderer, K. Jakob, and W. Gebhardt, in *Growth and Optical Properties of Wide-Gap II-VI Low Dimensional Semiconductors*, Vol. 20 of *NATO Advanced Study Institute, Series B: Physics*, edited by T. C. McGill, C. M. Sotomayor-Torres, and W. Gebhardt (Plenum, New York, 1989), p. 281.

[13] R. C. C. Leite and S. P. S. Porto, Phys. Rev. Lett. **17**, 10 (1966).

[14] A. Pinczuk and E. Burstein, Phys. Rev. Lett. **21**, 1073 (1968).

[15] R. M. Martin and T. C. Damen, Phys. Rev. Lett. **26**, 86 (1971).

[16] A. Cantarero, C. Trallero-Giner, and M. Cardona, Phys. Rev. B **39**, 8388 (1989).

[17] C. Trallero-Giner, A. Cantarero, and M. Cardona, Phys. Rev. B **40**, 4030 (1989).

[18] A. Cantarero, C. Trallero-Giner, and M. Cardona, Phys. Rev. B **40**, 12 290 (1989).

[19] C. Trallero-Giner, in *Proceedings of the 20th International Conference on the Physics of Semiconductors* (Ref. 11).

[20] A. A. Gogolin and E. I. Rashba, Solid State Commun. **19**, 1177 (1976).

[21] R. Zeyher, Phys. Rev. B **9**, 4439 (1974).

[22] V. I. Gavrilenko, D. Martinez, A. Cantarero, M. Cardona, and C. Trallero-Giner, Phys. Rev. B **42**, 11 718 (1990).

[23] A. Alexandrou, C. Trallero-Giner, A. Cantarero, and M. Cardona, Phys. Rev. B **40**, 1603 (1989).

[24] R. J. Elliott, Phys. Rev. **108**, 1384 (1957).

[25] H. Fröhlich, Adv. Phys. **3**, 325 (1954).

[26] L. D. Landau and E. M. Lifshitz, *Quantum Mechanics*, Vol. 3 of Course of Theoretical Physics (Pergamon, Oxford, 1977).

[27] I. S. Gradshteyn and I. M. Ryzhik, *Table of Integrals, Series and Products* (Academic, London, 1980).

[28] G. Arfken, *Mathematical Methods for Physicists* (Academic, New York, 1970).

[29] W. Gordon, Ann. Phys. **2**, 1031 (1929).

[30] *Landolt-Börnstein Tables*, edited by O. Madelung, H. Schulz, and H. Weiss (Springer, Berlin, 1982), Vol. III/17a.

[31] G. D. Mahan, *Many-Particle Physics* (Plenum, New York, 1983).

[32] A. A. Gogolin (unpublished).